ACS OMEGA

Article

http://pubs.acs.org/journal/acsodf

Preparation of Magnetic Carboxymethylchitosan Nanoparticles for Adsorption of Heavy Metal Ions

Thibaut V. J. Charpentier,*[†,∥] Anne Neville,[†] Joseph L. Lanigan,[†] Richard Barker,[†] Margaret J. Smith,[‡] and Thomas Richardson[§,∥]

[†]Institute of Functional Surfaces, Mechanical Engineering, Leeds University, Woodhouse Lane, Leeds LS2 9JT, U.K.

[‡]Centre for Textile Conservation and Technical Art History, University of Glasgow, Robertson Building, Dumbarton Road, Glasgow G11 6AQ, U.K.

[§]School of Physics, University of Bristol, Bristol BS8 1TL, U.K.

ABSTRACT: The remediation of metal and heavy metal contaminants from water ecosystems is a long-standing problem in the field of water management. The development of efficient, cost effective, and environmentally friendly natural polymer-based adsorbents is reported here. Magnetic chitosan (CS) and carboxymethylchitosan (CMC) nanocomposites have been synthesized by a simple one-step chemical coprecipitation method. The nanoparticles were assessed for the removal of Pb^{2+}, Cu^{2+}, and Zn^{2+} ions from aqueous solution. Kinetic and thermodynamic models were used to describe and understand the adsorption process of the ions onto the nanomaterials. The interactions between the ions and the biopolymer-based composites are reversible, which means that the nanoparticles can be regenerated in weakly acidic or EDTA containing solution without losing their activity and stability for water cleanup applications.

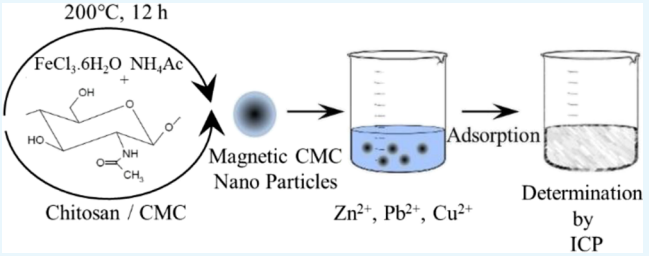

INTRODUCTION

The waste products of manufacturing processes of over three centuries of industrialization have had unintentional consequences, of which the long-term issues of environmental pollution, in both terrestrial and water systems, are widely reported. One major issue is the contamination of water ecosystems by toxic heavy metal ions; this has been a concern for many decades. The ability of metal ions to accumulate in the tissue of plants, fish, and mammals poses a serious threat to human health. This is both through bioaccumulation in the food chain and also because of their ability to bind to proteins and metabolites in living organisms.[1−4] Several techniques are available for heavy metal ion removal from water; typical technologies include ion-exchange, chemical precipitation, membrane filtration, electrochemical methods, and adsorption, to name only a few.[5] Among these, the use of biopolymers as adsorbents is especially attractive because of their low operational cost and high efficiency. This has contributed to the development of novel adsorbents in recent decades.[6,7] The use of biopolymer-based adsorbents, such as polysaccharides, offers biocompatibility and biodegradability advantages. This has led to their wider application in the water treatment industry.[8] Chitosan (CS) is a type of polyaminosaccharide synthesized from the deacetylation of chitin, a polysaccharide consisting predominantly of unbranched chains of β-(1 → 4)-2-acetoamido-2-deoxy-D-glucose. Chitin is the second most abundant polymer in nature after cellulose.[9] The amino and hydroxyl functional groups of CS are effective binding sites for metal ions. Carboxymethylchitosan (CMC) is reported to have a higher metal ion binding capacity than CS because of the increased chain flexibility and higher concentration of chelating groups.[10−13] Compared with conventional adsorbents, magnetic adsorbents offer the attractive benefit of allowing their straightforward separation and removal from water, with the use of an external magnetic field. In the current study, CS and CMC magnetite nanoparticles were prepared by a simple, one-step chemical coprecipitation method. The resulting nanocomposites were used as a tool for the rapid removal of heavy metal ions, such as copper (Cu(II)), lead (Pb(II)), and zinc (Zn(II)). The relationship between the adsorption capacity and the adsorption mechanisms was studied, and equilibrium data were analyzed using Langmuir and Freundlich isotherms.

EXPERIMENTAL SECTION

Materials. CS (low molecular weight), iron(III) chloride hexahydrate ($FeCl_3 \cdot 6H_2O$), ethylene glycol (EG), and ammonium acetate (NH_4Ac) were purchased from Sigma Aldrich. CMC was purchased from Santa Cruz Biotechnology, Inc. Pure water (18 MΩ cm) was obtained from a Milli-Q system (Millipore, Milford, MA, USA). Other chemicals were of analytical grade and were purchased from Sigma Aldrich.

Synthesis of CS and CMC Magnetic Nanoparticles. Colloidal nanoparticles were synthesized via a versatile solvothermal reaction reported by Fang et al.[14] with a

Received: May 2, 2016
Accepted: June 20, 2016
Published: July 8, 2016

DOI: 10.1021/acsomega.6b00035
ACS Omega 2016, 1, 77−83

modification. Briefly, 2.5 g of $FeCl_3 \cdot 6H_2O$, 4 g of NH_4Ac, and 1.2 g of CS or CMC were dissolved in EG (75 mL) aided by sonication for 30 min to form a clear solution. The solution was then transferred to a Teflon-lined autoclaved (100 mL) and heated at 200 °C for 12 h. After the reaction, the solution was cooled to room temperature and isolated with a magnet. The nanoparticles were thoroughly washed with distilled water and ethanol and then also stored in ethanol.

Adsorption Kinetic Studies. Aqueous solutions of heavy metal ions were prepared by dissolving $PbCl_2$, $CuCl_2$, and $ZnCl_2$ in distilled water to reach a final cation concentration of 100 $mg \cdot L^{-1}$. Sorption studies were then conducted by mixing 20 mg of CS and CMC magnetic nanoparticles into 20 mL of aqueous solutions of the desired heavy metal ion. The pH of the solution was then adjusted to 5.2 ± 0.5 below the pK_a of CS (~6.2). This ensures that the amine groups are protonated and the adsorption of metal ions onto (carboxymethyl) chitosan is optimal.[15] The resulting dispersions were shaken mechanically at 200 rpm at room temperature, and the effect of contact time was evaluated between 2 and 60 min. After 2, 5, 10, 30, and 60 min, 1 mL of solution was collected and the nanoparticles were removed by magnetic separation. The ion concentration was then analyzed by inductively coupled plasma atomic emission spectroscopy (ICP-OES). The adsorption capacities of CS and CMC magnetic nanoparticles q (mg/g) were calculated by eq 1

$$q = \frac{(C_0 - C_t) \times V}{w} \quad (1)$$

where C_0 and C_t denote the initial and final concentration of heavy metal ions in solution ($mg \cdot L^{-1}$), respectively. V denotes the volume of aqueous solution (L), and w is the mass of CS and CMC magnetic adsorbents (mg).

Adsorption Isotherm Studies. Adsorption isotherm studies describe the relationship between adsorbents and adsorbates at equilibrium.[16] Adsorption isotherms of Cu(II), Pb(II), and Zn(II) on CS and CMC magnetic nanoparticles were obtained by dispersing 0.1 g of magnetic adsorbent into 100 mL of heavy metal ion solution, with concentrations ranging from 100 to 700 $mg \cdot L^{-1}$. Adsorption isotherm experiments were conducted at pH 5.2 ± 0.5. Dispersions were shaken mechanically at 200 rpm at room temperature, and 1 mL of solution was withdrawn after 24 h. The colloidal nanoparticles were removed by magnetic separation, and the ion concentration was then established using ICP-OES analysis.

Regeneration Studies. For desorption experiments, 20 mg of CS and CMC nanoparticles previously loaded with Cu(II), Pb(II), and Zn(II) were collected and gently washed with distilled water to remove any unabsorbed metal ion, and then, 20 mL of EDTA solution (0.01 $mol \cdot L^{-1}$) was added. The samples were then shaken mechanically at 200 rpm at room temperature for 24 h for desorption to occur. Finally, colloidal nanoparticles were removed by magnetic separation, and the ion concentration was again analyzed using ICP-OES.

RESULTS AND DISCUSSION

Characterization of CS and CMC Magnetic Nanoparticles. The scanning electron microscopy (SEM) images of the CMC magnetic colloidal particles are given in Figure 1. The particles exhibit a uniform size of approximately 500 nm. Interestingly, the high-resolution transmission electron microscopy (HRTEM) images of the CMC magnetic particles (Figure 2) show fringes at the edges of the particles. The appearance of the colloidal particles is consistent with that of an agglomeration of smaller Fe_3O_4 precursors.

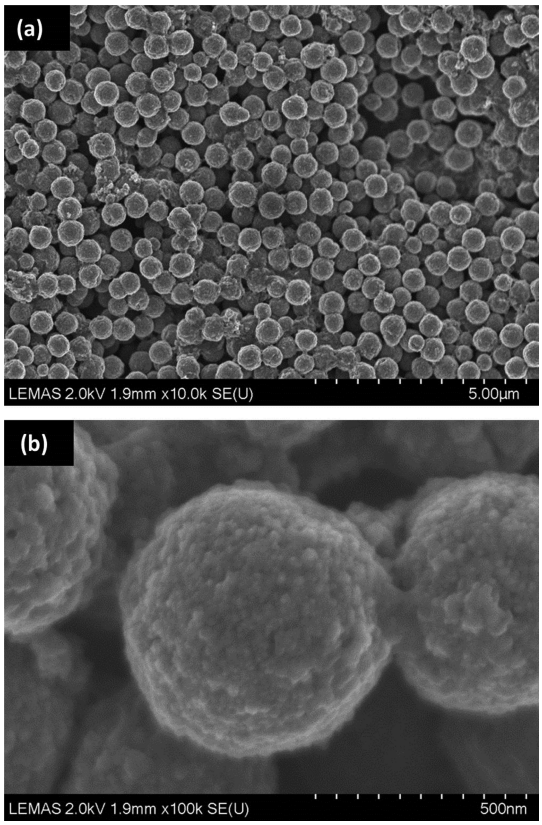

Figure 1. SEM micrographs of CMC magnetic nanoparticles at low (a) and high (b) resolution.

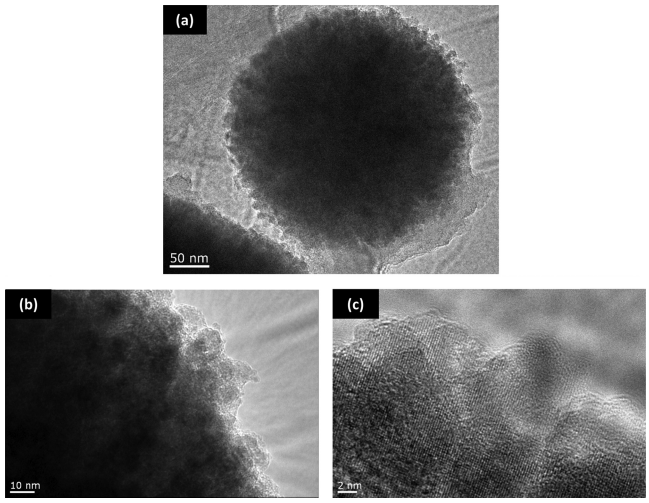

Figure 2. (a–c) HRTEM micrographs of CMC magnetic nanoparticles.

The structures of CS and CMC magnetite nanoparticles were characterized by X-ray diffraction (XRD) (Figure 3a). Six peaks that are characteristic of Fe_3O_4, namely, (220), (311), (400), (422), (511), and (440) were observed for all samples (JCPDS no. 75-1610). To confirm the presence of CS and CMC, FT-IR spectra of nanoparticle composites were examined and are shown in Figure 3b. The CS spectrum shows a strong peak at 3231 cm^{-1}, which is assigned to the N–H extension vibration

DOI: 10.1021/acsomega.6b00035
ACS Omega 2016, 1, 77–83

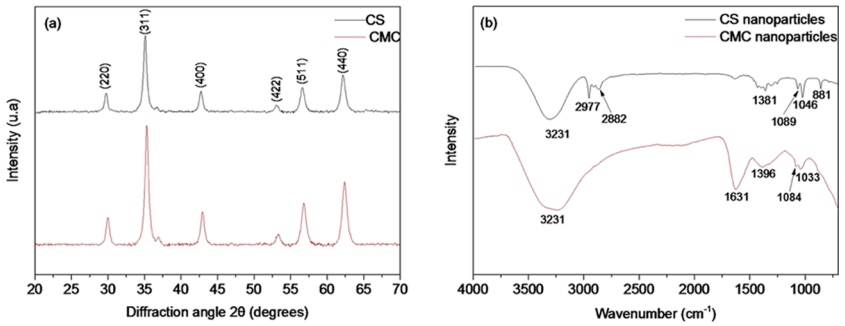

Figure 3. (a) XRD patterns of CS and CMC magnetite composite nanoparticles and (b) IR spectra of CS and CMC composite nanoparticles.

and O−H stretching vibration, as well as belonging to intermolecular hydrogen bonding, within the biopolymer. The signals at 2977 and 2882 cm^{-1} were assigned to the vibration of methyl and methylene C−H bonds, respectively. The peaks in 1089 and 1046 cm^{-1} corresponded to the bridge-O-stretch and C−O stretch, respectively.[17,18] The difference between CS and CMC spectra was the peaks obtained solely in the spectra of CMC at 1631 and 1396 cm^{-1}; this IR region is specific for the COO^- carboxylate group, and the peaks were attributed to the carboxylate C═O asymmetric stretching and the C═O symmetric stretching.[19]

Figure 4 shows the magnetization of CS and CMC magnetite nanoparticles as a function of the magnetic field at 300 K. The

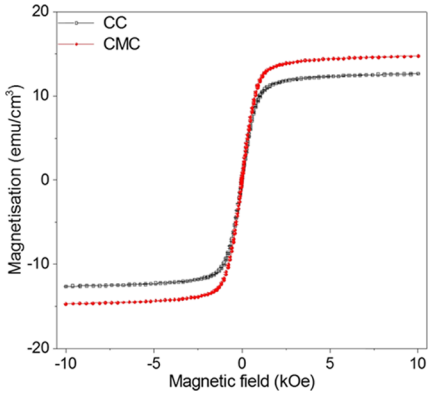

Figure 4. Magnetic hysteresis loops of CS and CMC magnetic nanoparticles at 300 K

measurements were obtained with a vibrating sample magnetometer (VSM) with an applied magnetic field ranging from −10 to 10 kOe. The absence of any significant remanence or coercivity in the magnetization curves suggests that the samples can be classified as paramagnetic. Moreover, the magnetic saturation of CS and CMC magnetite nanoparticles is 13 and 15 emu/g, respectively. Such magnetic properties mean that the nanoparticles are susceptible to an external magnetic field and can easily be separated from solution.

Kinetic Adsorption Study of Metal Ions on CS and CMC Nanocomposites. The adsorption performance of CS and CMC magnetic nanoparticles with metal ions was investigated by a batch equilibrium technique for contact times varying between 2 and 60 min. The results for Cu, Pb, and Zn ions are shown in Figure 5. The spontaneously high rate of metal ion uptake at short contact times was associated with the significant number of active sites available on the nanoparticles. However, as the contact times increase, metal ions progressively bind to these sites. The rate of sorption then slows down before reaching equilibrium after 60 min, as illustrated by the plateau on the curves in Figure 5. The adsorption capacity (q_e) of CS nanoparticles was in the following order: Pb(II) 88.5 $mg{\cdot}g^{-1}$ > Cu(II) 79.3 $mg{\cdot}g^{-1}$ > Zn(II) 61 $mg{\cdot}g^{-1}$. The performance of CMC nanocomposites was higher, with the following maximum ion uptakes: Pb(II) 107.5 $mg{\cdot}g^{-1}$ > Cu(II) 99 $mg{\cdot}g^{-1}$ > Zn(II) 75.8 $mg{\cdot}g^{-1}$. The increased sorption capacity of CMC was attributed to the availability of a large number of $-COO^-$ groups, which are able to coordinate to metal ions. To further investigate the adsorption mechanism and determine the sorption efficiency of the nanocomposites, the kinetic process was studied by fitting the experimental data to the kinetic models, presented in Table 1. According to the *R*-squared values of the regression analyses presented in Table 2, the pseudo-second-order model offers the best mathematical fit to describe the adsorption kinetics of Pb(II), Cu(II), and Zn(II) onto CS and CMC nanoparticles. Such kinetic models imply that chemisorption is likely to be the rate-limiting step of the adsorption process.[20,21]

Isotherm Adsorption Study. Figure 6 shows the adsorption equilibrium isotherm data obtained for Cu(II), Pb(II), and Zn(II) ions adsorbed onto CS and CMC nanocomposites. These adsorption isotherms allow for the amount of metal ions adsorbed (per unit weight of nanocomposites) to be correlated to the remaining concentration of metal ions in the aqueous phase at a given temperature under equilibria conditions. This type of data set is highly valuable to aid the understanding of the mechanism of adsorption, as well as to interpret the kinetics of the adsorption process. Figure 6 shows that the uptake capacity of the nanocomposites was found to increase with the equilibrium concentrations of the metal ions in solution, progressively reaching saturation of the adsorbent. The experimental data were fitted to the Langmuir and Freundlich models; these equations are shown in Table 3 and are commonly used for analyzing the nature of adsorbate−adsorbent interactions.[23,24]

According to the *R*-squared values of the regression analyses presented in Table 4, both Langmuir and Freundlich models fitted the experimental isotherm equilibrium data reasonably well, with R^2 values >0.927. According to these values, the Langmuir equation provided the best fit for the experimental data of the CS magnetic nanoparticles (for the three metal ions tested) in the entire range of concentrations studied. The Langmuir model assumes that the adsorbent surface has a finite number of binding sites of identical energy and that each adsorbate ion is located at a single site. The model suggests the formation of a monolayer of metal ions on the surface of CS nanoparticles. The maximum adsorption capacity (q_m) of CS

DOI: 10.1021/acsomega.6b00035
ACS Omega 2016, 1, 77−83

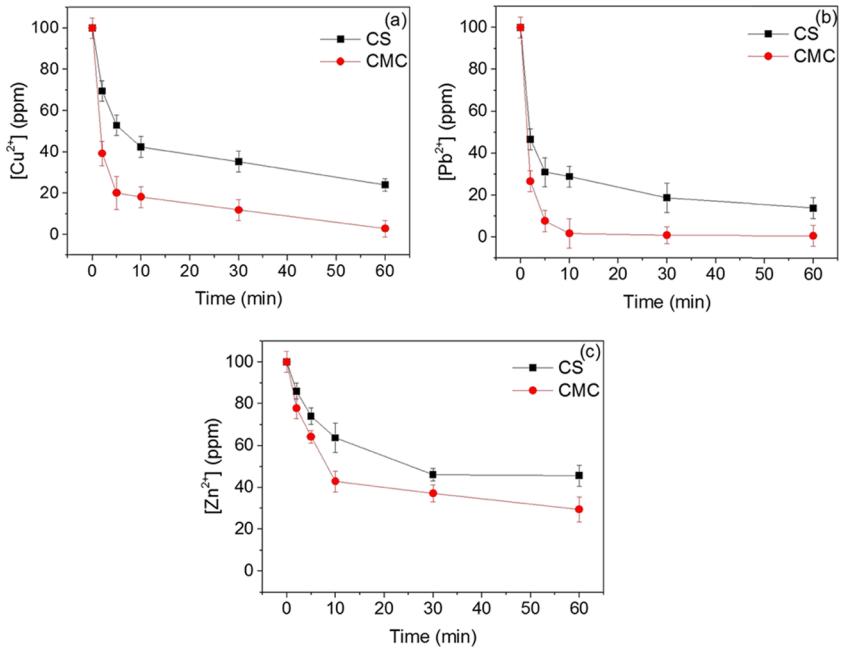

Figure 5. Effect of time on the adsorption of metal ions onto CS and CMC magnetic nanoparticles: (a) Cu(II), (b) Pb(II), and (c) Zn(II). The error bars represent standard errors.

Table 1. Mathematical Equations Applied in the Kinetic Adsorption Study of Metal Ions onto CS and CMC Nanoparticles[22]

kinetic models	linear equations	plot	calculated coefficient
pseudo-first-order[a]	$\ln(q_e - q_t) = \frac{\ln q_e - K_1 t}{2.303}$	$\ln(q_e - q_t)$ vs t	$K_1 = -\text{slope} \times 2.303$
			$q_e = e^{\text{intercept}}$
pseudo-second-order[b]	$\frac{1}{q_t} = \frac{1}{K_2 \times q_e^2} + \frac{t}{q_e}$	t/q_t vs t	$K_2 = \frac{\text{slope}^2}{\text{intercept}}$
			$q_e = \text{slope}^{-1}$

[a] K_1 (min^{-1}) and K_2 ($\text{g·mg}^{-1}\text{·min}^{-1}$) denote the order rate constants for the pseudo-first-order; q_t is the adsorption amount of metal ions at time t (mg·g^{-1}), and q_e is the equilibrium adsorption amount (mg·g^{-1}), whereas t gives the contact time (min). [b] K_1 (min^{-1}) and K_2 ($\text{g·mg}^{-1}\text{·min}^{-1}$) denote the order rate constants for the pseudo-second-order; q_t is the adsorption amount of metal ions at time t (mg·g^{-1}), and q_e is the equilibrium adsorption amount (mg·g^{-1}), whereas t gives the contact time (min).

Table 2. Kinetic Parameters for Cu(II), Pb(II), and Zn(II) Ion Adsorption

		pseudo-first-order			pseudo-second-order		
metal	material	q_e	K_1	R^2	q_e	K_2	R^2
Pb(II)	CS nanoparticles	28.7	9.8×10^{-2}	0.969	88.5	6.3×10^{-3}	0.999
	CMC nanoparticles	20.58	1.0×10^{-1}	0.871	107.5	1.0×10^{-2}	0.998
Cu(II)	CS nanoparticles	43.2	9.7×10^{-2}	0.964	79.3	3.2×10^{-3}	0.995
	CMC nanoparticles	32.2	1.1×10^{-1}	0.947	99.0	5.6×10^{-3}	0.998
Zn(II)	CS nanoparticles	37.4	7.9×10^{-2}	0.816	61.0	2.6×10^{-2}	0.996
	CMC nanoparticles	42.0	8.4×10^{-2}	0.901	75.8	2.7×10^{-3}	0.997

nanocomposites was Pb(II) 141 mg·g^{-1} > Cu(II) 123 mg·g^{-1} > Zn(II) 88 mg·g^{-1}. For the CMC nanocomposites, the maximum adsorption capacity was significantly higher for the three metal ions in the order Pb(II) 243 mg·g^{-1} > Cu(II) 232 mg·g^{-1} > Zn(II) 131 mg·g^{-1}. The Freundlich model was found to be more accurate when describing the adsorption of metal ions on CMC nanocomposites. Freundlich isotherms represent an empirical model employed to describe the equilibrium on a heterogeneous surface; they do not assume a monolayer capacity as in the case of the Langmuir model.[26] Freundlich isotherms suggest the presence of different binding sites on the adsorbent, which is in agreement with the chemical structure of CMC. Both carboxylate $-COO^-$ and amino $-NH_2$ groups can participate in the metal-ion binding process. The value of $1/n$ (Freundlich model) can be used to predict the binding affinity between the sorbent and the sorbate[27] with small values, implying stronger interactions between sorbents and metal ions. From Table 4, the values of n for Pb(II) are larger than those for Cu(II) and Zn(II), suggesting stronger binding interactions between Pb(II) and the active sites of CMC nanocomposites.

The adsorption capacity of the synthesized CS and CMC magnetic nanoparticles toward heavy metal ions is compared with those reported, as shown in Table 5. The maximum

DOI: 10.1021/acsomega.6b00035
ACS Omega 2016, 1, 77−83

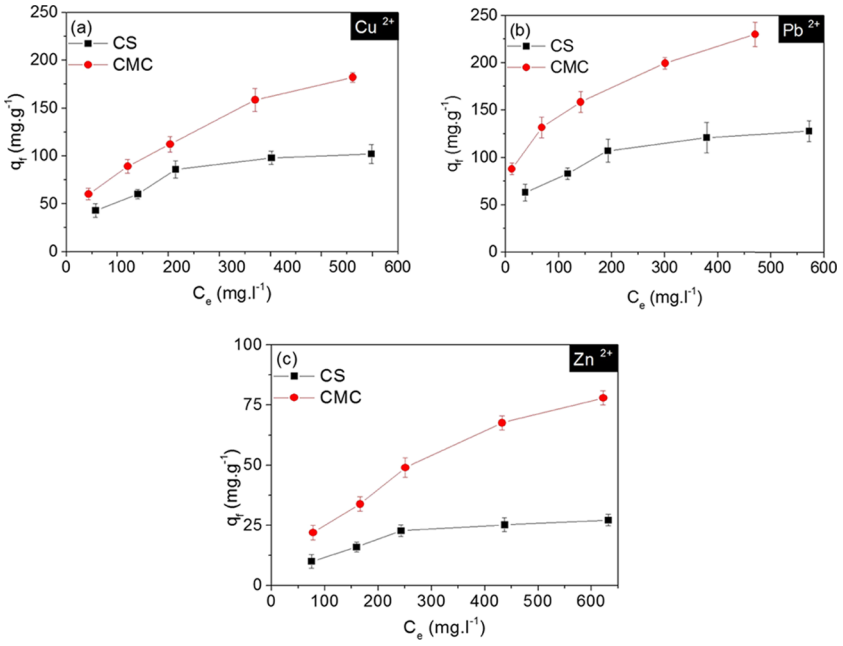

Figure 6. Adsorption isotherms of CS and CMC magnetic nanoparticles in (a) Cu(II), (b) Pb(II), and (c) Zn(II) aqueous solutions. The error bars represent standard errors.

Table 3. Mathematical Equations Applied in Adsorption Isotherm Study of Metal Ions onto CS and CMC Nanoparticles[25]

models	linear equations	plot	calculated coefficient
Langmuir[a]	$\frac{C_e}{q_e} = \frac{1}{q_m K_L} + \frac{C_e}{q_f}$	C_e/q_e vs C_e	$K_L = \frac{\text{slope}}{\text{intercept}}$
			$q_m = \text{slope}^{-1}$
Freundlich[b]	$\log q_e = \log K_F + \frac{\log C_e}{n}$	$\log q_e$ vs $\log C_e$	$K_F = 10^{\text{intercept}}$
			$n = \text{slope}^{-1}$

[a] q_e and C_e denotes the amount adsorbed (mg·g^{-1}) and adsorbate concentration in solution (mg·L^{-1}) at equilibrium, respectively. K_L is the Langmuir constant (L·mg^{-1}), and q_m denotes the maximum adsorption capacity of the monolayer formed on the adsorbent. [b] K_f and n denote the Freundlich isotherm constants, indicating the adsorption capacity (mg·g^{-1}) and adsorption intensity (dimensionless), respectively.

capacity of CMC magnetic nanoparticles is certainly comparable and possibly even higher than that of other CS-based adsorbents for the three metal ions tested. This is with the exceptions of CS hydroxyapatite nanocomposite beads and CS-coated mesoporous calcium silicate hydrate microspheres because of the high specific surface area of the microspheres.

Table 5. Comparison of Adsorption Capacities of CS and CMC Magnetic Nanoparticles Reported Herein toward Heavy Metal Ions with Those Reported in the Literature

adsorbent	adsorption capacity (mg·g^{-1}) Pb^{2+}	Cu^{2+}	Zn^{2+}	references
CS mesoporous microspheres	796	425	400	28
CS magnetite beads	63			29
CS multifunctional nanocomposite	70	66		30
magnetic CS/cellulose microspheres	46	88		31
CS hydroxyapatite nanocomposite	1385			32
CS rectorite nanocomposite		21		33
CS and CMC magnetite nanoparticles	**243**	**232**	**131**	**This work**

Regeneration Studies. Desorption experiments are of paramount importance for the recovery of the metal ions to help understand the adsorption process of the adsorbates. In the current study, the nanoparticles were regenerated by stripping the sorbed metal ions using EDTA chelation; such a procedure has previously been found to desorb metal ions from CS in a superior manner to using a solution of HCl.[33−35] Figure 7 shows the regeneration of the nanocomposites over three successive cycles of adsorption and desorption. The results show that the magnetic nanocomposites release the adsorbed

Table 4. Isotherm Parameters of Metal Ion Adsorption on CS and CMC Nanocomposites

metal	material	Langmuir isotherm q_m	K_L	R^2	Freundlich isotherm $1/n$	K_f	R^2
Pb(II)	CS nanoparticles	141	1.6×10^{-2}	0.996	0.27	23.9	0.972
	CMC nanoparticles	243	1.9×10^{-2}	0.983	0.26	45.1	0.995
Cu(II)	CS nanoparticles	123	9.0×10^{-3}	0.990	0.39	9.3	0.939
	CMC nanoparticles	232	6.3×10^{-3}	0.971	0.44	11.3	0.993
Zn(II)	CS nanoparticles	88	6.0×10^{-3}	0.988	0.47	3.5	0.927
	CMC nanoparticles	131	2.3×10^{-3}	0.977	0.63	1.4	0.990

DOI: 10.1021/acsomega.6b00035
ACS Omega 2016, 1, 77−83

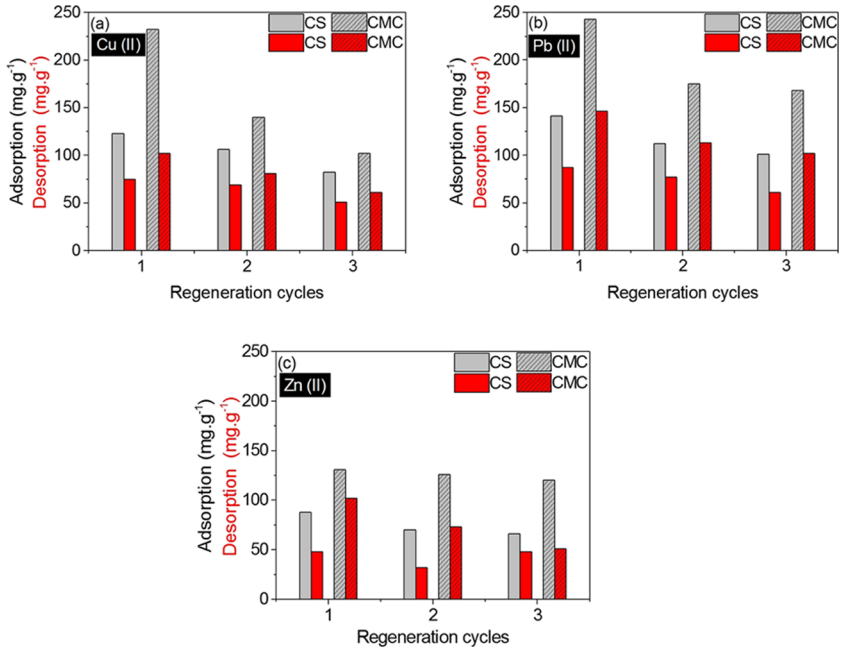

Figure 7. Adsorption−desorption cycles of (a) Cu(II), (b) Pb(II), and (c) Zn(II) onto CS and CMC magnetite nanocomposites.

metal ions with regeneration efficiency above 60% based on the adsorption capacity in each cycle. Despite the overall adsorption capacity reducing slightly after each cycle, the adsorption capacity of the magnetic nanoparticles remains high, which suggests a limited number of irreversible sites on the surfaces of the synthesized nanocomposites that are not recovered when using the EDTA desorption solution. Interestingly, the capacity loss observed was larger for nanoparticles loaded with Pb(II) and Cu(II) than that for nanoparticles loaded with Zn(II). It is likely that the higher binding affinity between the sorbent and Pb(II) and Cu(II) highlighted in the isotherm adsorption studies somewhat limits the stripping effect of the EDTA solution, which tends to moderately reduce their loading ability after successive regeneration cycles.

CONCLUSION

CS and CMC magnetic nanocomposites were synthesized using a simple one-step chemical coprecipitation method. The nanoparticles provide an efficient, fast, and environmentally friendly approach for the removal of the metal ions Cu(II), Pb(II), and Zn(II) from aqueous solutions. The current work shows that the binding capacity of the nanoparticles to metal ions is comparable or even higher than that of other CS-based adsorbents. In addition to the amine groups, the presence of a carboxylic moiety on CMC nanoparticles is likely to offer additional binding sites, which considerably enhance their loading capacity in comparison to the CS nanoparticles. This mechanism is in agreement with the good fitting of the experimental data with the Freundlich adsorption isotherm. Moreover, the magnetic properties of the nanoparticles when coupled to their regenerative performances make them a potential, efficient, and cost-effective tool for heavy metal ion removal for water treatment industries.

AUTHOR INFORMATION

Corresponding Author

*E-mail: T.Charpentier@leeds.ac.uk.

Author Contributions

‖T.V.J.C. and T.R. contributed equally to this work.

Author Contributions

The manuscript was written through contributions of all authors. All authors have given approval to the final version of the manuscript.

Notes

The authors declare no competing financial interest.

REFERENCES

(1) Liu, D.; Li, Z.; Zhu, Y.; Li, Z.; Kumar, R. Recycled chitosan nanofibril as an effective Cu(II), Pb(II) and Cd(II) ionic chelating agent: Adsorption and desorption performance. *Carbohydr. Polym.* **2014**, *111*, 469−476.

(2) Liphadzi, M. S.; Kirkham, M. B. Availability and plant uptake of heavy metals in EDTA-assisted phytoremediation of soil and composted biosolids. *J. S. Afr. Bot.* **2006**, *72*, 391−397.

(3) Crini, G. Recent developments in polysaccharide-based materials used as adsorbents in wastewater treatment. *Prog. Polym. Sci.* **2005**, *30*, 38−70.

(4) Kul, A. R.; Koyuncu, H. Adsorption of Pb(II) ions from aqueous solution by native and activated bentonite: Kinetic, equilibrium and thermodynamic study. *J. Hazard. Mater.* **2010**, *179*, 332−339.

(5) Aragay, G.; Pons, J.; Merkoçi, A. Recent Trends in Macro-, Micro-, and Nanomaterial-Based Tools and Strategies for Heavy-Metal Detection. *Chem. Rev.* **2011**, *111*, 3433−3458.

(6) Mudhoo, A.; Garg, V. K.; Wang, S. Removal of heavy metals by biosorption. *Environ. Chem. Lett.* **2012**, *10*, 109−117.

(7) Lim, A. P.; Aris, A. Z. A review on economically adsorbents on heavy metals removal in water and wastewater. *Rev. Environ. Sci. Bio/Technol.* **2014**, *13*, 163−181.

(8) Wan Ngah, W. S.; Teong, L. C.; Hanafiah, M. A. K. M. Adsorption of dyes and heavy metal ions by chitosan composites: A review. *Carbohydr. Polym.* **2011**, *83*, 1446−1456.

(9) Wan Ngah, W. S.; Ariff, N. F. M.; Hashim, A.; Hanafiah, M. A. K. M. Malachite Green Adsorption onto Chitosan Coated Bentonite Beads: Isotherms, Kinetics and Mechanism. *Clean: Soil, Air, Water* **2010**, *38*, 394−400.

(10) Muzzarelli, R. A. A.; Weckx, M.; Filippini, O.; Sigon, F. Removal of trace metal ions from industrial waters, nuclear effluents and

DOI: 10.1021/acsomega.6b00035
ACS Omega 2016, 1, 77−83

drinking water, with the aid of cross-linked *N*-carboxymethyl chitosan. *Carbohydr. Polym.* **1989**, *11*, 293−306.
(11) Varma, A. J.; Deshpande, S. V.; Kennedy, J. F. Metal complexation by chitosan and its derivatives: a review. *Carbohydr. Polym.* **2004**, *55*, 77−93.
(12) Guibal, E. Interactions of metal ions with chitosan-based sorbents: a review. *Sep. Purif. Technol.* **2004**, *38*, 43−74.
(13) Wan Ngah, W. S.; Liang, K. H. Adsorption of Gold(III) Ions onto Chitosan and *N*-Carboxymethyl Chitosan: Equilibrium Studies. *Ind. Eng. Chem. Res.* **1999**, *38*, 1411−1414.
(14) Fang, C.; Xiong, Z.; Qin, H.; Huang, G.; Liu, J.; Ye, M.; Feng, S.; Zou, H. One-pot synthesis of magnetic colloidal nanocrystal clusters coated with chitosan for selective enrichment of glycopeptides. *Anal. Chim. Acta* **2014**, *841*, 99−105.
(15) Schmuhl, R.; Krieg, H. M.; Keizer, K. Adsorption of Cu(II) and Cr(VI) ions by chitosan : kinetics and equilibrium studies. *Water SA* **2001**, *27*, 1−8.
(16) Yu, B.; Xu, J.; Liu, J.-H.; Yang, S.-T.; Luo, J.; Zhou, Q.; Wan, J.; Liao, R.; Wang, H.; Liu, Y. Adsorption behavior of copper ions on graphene oxide−chitosan aerogel. *J. Environ. Chem. Eng.* **2013**, *1*, 1044−1050.
(17) Brugnerotto, J.; Lizardi, J.; Goycoolea, F. M.; Argüelles-Monal, W.; Desbrières, J.; Rinaudo, M. An infrared investigation in relation with chitin and chitosan characterization. *Polymer* **2001**, *42*, 3569−3580.
(18) Shigemasa, Y.; Matsuura, H.; Sashiwa, H.; Saimoto, H. Evaluation of different absorbance ratios from infrared spectroscopy for analyzing the degree of deacetylation in chitin. *Int. J. Biol. Macromol.* **1996**, *18*, 237−242.
(19) Safee, N. H. A.; Abdullah, M. P.; Othman, M. R. Carboxymethyl chitosan−Fe_3O_4 nanoparticles: synthesis and characterization. *Malays. J. Anal Sci.* **2010**, *14*, 63−68.
(20) Lin, Y.-F.; Chen, H.-W.; Chien, P.-S.; Chiou, C.-S.; Liu, C.-C. Application of bifunctional magnetic adsorbent to adsorb metal cations and anionic dyes in aqueous solution. *J. Hazard. Mater.* **2011**, *185*, 1124−1130.
(21) Monier, M.; Abdel-Latif, D. A. Preparation of cross-linked magnetic chitosan-phenylthiourea resin for adsorption of Hg(II), Cd(II) and Zn(II) ions from aqueous solutions. *J. Hazard. Mater.* **2012**, *209−210*, 240−249.
(22) Hao, Y.-M.; Man, C.; Hu, Z.-B. Effective removal of Cu(II) ions from aqueous solution by amino-functionalized magnetic nanoparticles. *J. Hazard. Mater.* **2010**, *184*, 392−399.
(23) Wan Ngah, W. S.; Kamari, A.; Koay, Y. J. Equilibrium and kinetics studies of adsorption of copper(II) on chitosan and chitosan/PVA beads. *Int. J. Biol. Macromol.* **2004**, *34*, 155−161.
(24) Justi, K. C.; Fávere, V. T.; Laranjeira, M. C. M.; Neves, A.; Peralta, R. A. Kinetics and equilibrium adsorption of Cu(II), Cd(II), and Ni(II) ions by chitosan functionalized with 2[-bis-(pyridylmethyl)aminomethyl]-4-methyl-6-formylphenol. *J. Colloid Interface Sci.* **2005**, *291*, 369−374.
(25) Foo, K. Y.; Hameed, B. H. Insights into the Modeling of Adsorption Isotherm Systems. *Chem. Eng. J.* **2010**, *156*, 2−10.
(26) Abou El Fadl, F. I. Radiation grafting of ionically crosslinked alginate/chitosan beads with acrylic acid for lead sorption. *J. Radioanal. Nucl. Chem.* **2014**, *301*, 529−535.
(27) Lin, K.; Pan, J.; Chen, Y.; Cheng, R.; Xu, X. Study the adsorption of phenol from aqueous solution on hydroxyapatite nanopowders. *J. Hazard. Mater.* **2009**, *161*, 231−240.
(28) Zhao, J.; Zhu, Y.-J.; Wu, J.; Zheng, J.-Q.; Zhao, X.-Y.; Lu, B.-Q.; Chen, F. Chitosan-coated mesoporous microspheres of calcium silicate hydrate: Environmentally friendly synthesis and application as a highly efficient adsorbent for heavy metal ions. *J. Colloid Interface Sci.* **2014**, *418*, 208−215.
(29) Tran, H. V.; Tran, L. D.; Nguyen, T. N. Preparation of chitosan/magnetite composite beads and their application for removal of Pb(II) and Ni(II) from aqueous solution. *Mater. Sci. Eng., C* **2010**, *30*, 304−310.
(30) Alsabagh, A. M.; Fathy, M.; Morsi, R. E. Preparation and characterization of chitosan/silver nanoparticle/copper nanoparticle/carbon nanotube multifunctional nano-composite for water treatment: heavy metals removal; kinetics, isotherms and competitive studies. *RSC Adv.* **2015**, *5*, 55774−55783.
(31) Luo, X.; Zeng, J.; Liu, S.; Zhang, L. An effective and recyclable adsorbent for the removal of heavy metal ions from aqueous system: Magnetic chitosan/cellulose microspheres. *Bioresour. Technol.* **2015**, *194*, 403−406.
(32) Saber-Samandari, S.; Saber-Samandari, S.; Nezafati, N.; Yahya, K. Efficient removal of lead(II) ions and methylene blue from aqueous solution using chitosan/Fe-hydroxyapatite nanocomposite beads. *J. Environ. Manage.* **2014**, *146*, 481−490.
(33) Zeng, L.; Chen, Y.; Zhang, Q.; Guo, X.; Peng, Y.; Xiao, H.; Chen, X.; Luo, J. Adsorption of Cd(II), Cu(II) and Ni(II) ions by cross-linking chitosan/rectorite nano-hybrid composite microspheres. *Carbohydr. Polym.* **2015**, *130*, 333−343.
(34) Singh, K.; Suri, R.; Tiwary, A. K.; Rana, V. Chitosan films: crosslinking with EDTA modifies physicochemical and mechanical properties. *J. Mater. Sci.: Mater. Med.* **2012**, *23*, 687−695.
(35) Crini, G.; Morin-Crini, N.; Fatin-Rouge, N.; Déon, S.; Fievet, P. Metal removal from aqueous media by polymer-assisted ultrafiltration with chitosan. *Arabian J. Chem.* **2014**, DOI: 10.1016/j.arabjc.2014.05.020.

DOI: 10.1021/acsomega.6b00035
ACS Omega 2016, 1, 77−83